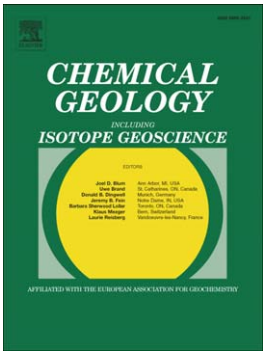

Mantle-derived helium in hot springs of the cordillera Blanca, Peru: Implications for mantle-to-crust fluid transfer in a flat-slab subduction setting

Dennis L. Newell, Micah J. Jessup, David R. Hilton, Colin Shaw, Cameron Hughes

PII: S0009-2541(15)30050-4
DOI: doi: 10.1016/j.chemgeo.2015.10.003
Reference: CHEMGE 17712

To appear in: *Chemical Geology*

Received date: 24 August 2015
Revised date: 30 September 2015
Accepted date: 1 October 2015

Please cite this article as: Newell, Dennis L., Jessup, Micah J., Hilton, David R., Shaw, Colin, Hughes, Cameron, Mantle-derived helium in hot springs of the cordillera Blanca, Peru: Implications for mantle-to-crust fluid transfer in a flat-slab subduction setting, *Chemical Geology* (2015), doi: 10.1016/j.chemgeo.2015.10.003

Mantle-derived helium in hot springs of the Cordillera Blanca, Peru: implications for mantle-to-crust fluid transfer in a flat-slab subduction setting

Dennis L. Newell[1*], Micah J. Jessup[2], David R. Hilton[3], Colin Shaw[4], and Cameron Hughes[2]

[1]Corresponding author, Department of Geology, 4505 Old Main Hill, Utah State University, Logan, UT 84322; dennis.newell@usu.edu; 435-797-0479*

[2]Department of Earth and Planetary Sciences, University of Tennessee, Knoxville, Knoxville, TN

[3]Scripps Institution of Oceanography, UC San Diego, La Jolla, CA 92093

[4]Department of Earth Sciences, Montana State University, Bozeman, MT

ABSTRACT

Fault-controlled hot springs in the Cordillera Blanca, Peru provide geochemical evidence of mantle-derived fluids in a modern flat-slab subduction setting. The Cordillera Blanca is a ~200 km-long mountain range contains the highest peaks in the Peruvian Andes, located in an amagmatic reach of the Andean arc. The Cordillera Blanca detachment defines the southwestern edge of the range and records a progression of top-down-to-the-west ductile shear to brittle normal faulting since ~5 Ma. Hot springs, recording temperatures up to 78 °C, issue along this fault zone and are CO_2-rich, near neutral, alkaline-chloride to alkaline-carbonate waters, with elevated trace metal contents including arsenic (≤11 ppm). Water $\delta^{18}O_{SMOW}$ (-14.2 to -4.9 ‰) and δD_{SMOW} (-106.2 to -74.3 ‰), trends in elemental chemistry, and cation geothermometry collectively demonstrate mixing of hot (200–260°C) saline fluid with cold meteoric water along the fault. Helium isotope ratios ($^3He/^4He$) for dissolved gases in the waters range from 0.62 to 1.98 R_A (where R_A = air $^3He/^4He$), indicating the presence of up to 25% mantle–derived helium. Given the long duration since and large distance to active magmatism in the region, and the possible presence of a tear in the flat slab south of the Cordillera Blanca, we suggest that mantle helium may originate from asthenosphere entering the slab tear, or from the continental mantle-lithosphere, mobilized by metasomatic fluids derived from slab dehydration.

Keywords: mantle helium, flat slab, Cordillera Blanca, hydrothermal fluids, Peruvian Andes

1. INTRODUCTION

Thermal springs in continental arc settings provide a direct window into the source and cycling of aqueous fluids and volatiles in subduction zones. Geochemical and isotopic data from

hot springs and fumaroles can preserve a modern record of slab- and mantle-derived fluid sources (e.g., Sano and Marty, 1995; Fischer et al., 2002; Hilton et al., 2002; Zimmer et al., 2004) in contrast to information inferred from geochemical studies of exhumed arc rocks and xenoliths that constrain the nature of fossil fluids in subduction zones (e.g., Scambelluri and Philippot, 2001; Lee, 2005). Geophysical imaging at these margins, when available, can offer complementary information on the geometry of the subduction zone and possible locations of melts and/or other fluids. Such geophysical studies identify present-day fluids as well as structures that may control their distribution and migration through the crust to the surface, such as deep crustal faults, detachments near the brittle-ductile transition, and fracture meshes in the lower ductile crust (Zandt et al., 2003; Wannamaker et al., 2009; Meqbel et al., 2014).

Flat slabs represent a distinct type of low-angle subduction characterized by an absence of active continental arc magmatism and thus are unique settings to investigate subduction zone fluids. Most continental arcs involve normal (steep) subduction, slab dehydration, and release of fluids to the overlying asthenospheric wedge that leads to magmatism (e.g., Peacock, 1990). In contrast, direct contact between the down-going oceanic and overlying lithosphere during "flat-slab" subduction eliminates the asthenospheric wedge and inhibits melting and arc volcanism (Pilger, 1981). Slab-to-lithosphere fluid (water and volatiles) transfer in this setting persists and is invoked as an important mechanism for fertilizing and altering the rheology of the continental lithosphere (e.g., Humphreys et al., 2003; Lee, 2005; Hoke and Lamb, 2007; Jones et al., 2015). Approximately 10% of present-day convergent margins exhibit low-angle subduction segments (Gutscher et al., 2000); however, only three of these, located along the Andean Arc, are described as well-established flat slabs (Pérez-Gussinyé et al., 2008). Addtionally, recent geophysical investigations of the Peruvian flat slab suggest that part of the slab is tearing and the

downgoing plate is resuming a normal steep subduction angle (Antonijevic et al., 2015), indicating more heterogeneity in the slab geometry than previously documented in other modern flat slabs. To date, little geochemical data is available on the nature of aqueous fluids and volatiles in modern flat-slab settings, making it challenging to evaluate the significance of fluids in this phase of the subduction cycle.

Mantle and slab-derived volatiles released to the continental lithosphere are subject to significant modification by crustal processes such as mixing, degassing, and mineralization (e.g., van Soest et al., 1998; Ray et al., 2009). Thus, most studies of volatile geochemistry at convergent margins focus on active arcs and target thermal systems proximal to volcanic centers that display relatively low crustal modification to distinguish and characterize fluids derived from the mantle wedge and subducting slab. Applying these geochemical tools to thermal systems at arcs that are amagmatic, such as present-day flat-slab settings, is particularly challenging owing to the potential for significant crustal overprinting. However, we suggest that by carefully addressing the crustal geochemical overprint, it is possible to effectively interpret volatile cycling in settings lacking active magmatism.

In this contribution, we present new He isotope ($^3He/^4He$) results from thermal springs issuing along a 200-km-long normal fault that bounds the highest peaks of the Peruvian Andes in the Cordillera Blanca. These data, in combination with supporting geochemical and stable isotope analyses, provide direct evidence for present-day circulation of mantle-derived fluids in an amagmatic flat-slab setting. We explore the possible origins of these fluids including mobilization of mantle He from the continental mantle lithosphere by slab-derived metasomatic fluids, and asthenosphere-derived fluids associated with the inferred tear in the Peruvian flat slab (Antonijevic et al., 2015) which may extend northward under the Cordillera Blanca.

2. GEOLOGIC SETTING

2.1. Subduction Zone Style and Arc Volatiles in the Andes

Shallowing of the subducting slab and eventual establishment of a flat slab is postulated to have occurred along several segments of the Andean arc, supported by observations of the eastward (down dip) migration and eventual cessation of magmatism (e.g., Hoke and Lamb, 2007), the presence of adakitic magmatism (Kay and Abbruzzi, 1996), and by geophysical imaging of present-day slabs (Gutscher et al., 2000; Antonijevic et al., 2015). Presently, there are three segments of flat-slab subduction that are characteristically amagmatic, separated by segments with steeper 'normal' subduction angles associated with active magmatism (Ramos and Folguera, 2009) (Fig. 1). These flat-slab segments include the Bucaramanga segment north of 5 °N (not shown), the Peruvian segment between 5 and 15 °S, and the Chilean segment located from 27-33.5 °S (Gutscher et al., 2000).

Recent 3D geophysical investigations of the Peruvian flat slab suggest that part of the slab north of the Nazca ridge may be sinking and tearing today (Fig. 1 contours), possibly capturing a transition back to normal steep subduction (Antonijevic et al., 2015). The northern end of these investigations is located approximately 1 - 2° south of the Cordillera Blanca, so it is unknown if this tear extends beneath our study region. Prior 2D seismic tomography of the Peruvian flat slab noted a 'sag' region between the Nazca ridge and Inca Plateau (Gutscher et al., 2000), broadly beneath the Cordillera Blanca, but their survey lacks the resolution to resolve a tear in the slab.

The transition between steep and flat-slab subduction zones in the Andes is exemplified in the Altiplano – Puna plateau (Fig. 1). Here, past normal arc magmatism shifted to an amagmatic flat-slab phase at ~35 Ma that persisted for approximately 10 million years before returning to steeper subduction and the magmatic activity observed today (Hoke and Lamb, 2007). During flat-slab subduction, dehydration of the slab is postulated to have fertilized and weakened the overlying lithosphere leading to continental mantle lithosphere delamination and uplift of the plateau (Hoke and Lamb, 2007). Antonijevic et al. (2015) document a potential present-day transition from flat to steep subduction in the Peruvian segment, and postulate that this tear initiated due to the loss of buoyancy in the slab following the passing of the Nazca ridge as it subducted obliquely beneath South America. However, it is unknown if similar geodynamic processes impacted the Altiplano – Puna plateau region in the past, and it is unknown what role fluids may have in the observed foundering of the Peruvian slab.

Detailed volatile studies constrain the source of Andean arc fluids along the magmatically active segments of Ecuador, Bolivia, and Chile (Fig. 1, Table S1). Helium isotope ratios track the mixing of upper mantle-derived helium (8 R_A, the measured $^3He/^4He$ ratio reported relative to the air ratio of 1.4×10^{-6}) and radiogenic He characteristic of the crust (0.02 - 0.1 R_A) (Ozima and Podosek, 1983). The largest mantle contributions are found at thermal features associated with active volcanoes. However, significant He isotope ratio variability between thermal features is observed due to admixtures between meteoric groundwater and crustal contamination of mantle-derived melts. In contrast, studies reporting helium isotope ratios and/or other volatile data from thermal springs within the flat-slab segments of the Andean arc are very limited. Hilton et al. (1993) report 1.45 R_A from Baños Toros located in the Chilean flat-slab segment (Fig. 1). Assuming mixing between crustal (0.02 R_A) and asthenospheric mantle (8 R_A) helium sources,

this equates to approximately 18% mantle-derived helium. Helium isotope ratios are not reported for thermal springs along the Bucaramanga or Peruvian flat-slab segments. Peruvian Geological Survey reports (e.g., Huaccan, 2000) provide elemental chemistry from hot springs throughout Peru, but no isotopic or volatile data are reported.

2.2. The Cordillera Blanca

The Cordillera Blanca (CB) massif is a northwest-trending range with numerous peaks between 5 and 6.7 km in elevation (Fig. 2). It is composed of the CB batholith, which was emplaced into shallow crustal levels (3 kbar) at 8.0 ± 0.2 Ma (Atherton and Sanderson, 1987). A 200-km-long extensional detachment fault that bounds the southwestern margin of the range (Fig. 2) preserves deformation during "top-down-to-the-southwest" sense of shear (McNulty and Farber, 2002). Together with steeper, brittle normal faults, these features have accommodated syn-convergent extension in the highest elevations of Peru since ~5.4 Ma (Giovanni et al., 2010). Hot springs issue along the Cordillera Blanca detachment fault system. Two springs emanate from the main detachment fault near the northern end of the CB, and others issue from mapped or inferred faults in the hanging wall of the detachment (Fig. 2).

3. METHODS AND MATERIALS

3.1. Water and dissolved gas sampling

Samples were collected as close to the spring sources as possible. Water samples were collected in 60 and 125 ml high-density polyethylene bottles. Samples for carbonate alkalinity and anion analysis were collected unfiltered with no headspace. Samples for cation analysis were field filtered using 0.45 μm syringe filters and were preserved with concentrated trace metal grade HNO_3. Samples for stable oxygen and hydrogen isotope ratio determination were collected

in 12 ml glass septa vials with no headspace. Water or gas samples for He isotope analysis were collected in 12 in. × 3/8 in. OD (~30 cm × 0.95 cm) copper tubes that were sealed with refrigeration clamps after purging with spring waters/gases. Gas splits for carbon stable isotope analysis of total dissolved CO_2 were prepared during the gas purification and extraction procedure used for helium isotopes. He and CO_2 collection protocols follow closely those described in Hilton et al. (2002).

3.2. Chemical and Isotopic Analysis

Water temperature, pH and conductivity were measured using an Oakton pH/cond/T portable meter. Major and trace element concentrations in spring waters were analyzed at the Utah State University (USU) Water Research Laboratory using a Dionex Ion Chromatograph (anions) and Agilent ICP-MS (cations). Total alkalinity was measured by manual colorimetric titration.

The $\delta^{13}C$ values of the total dissolved CO_2 were measured at the Scripps Institution of Oceanography using a ThermoFinnigan DeltaPlus isotope ratio mass spectrometer (IRMS). Result are reported in per mil (‰) relative to the PDB scale with an uncertainty of ±0.1 ‰ based on repeat analysis of NBS carbonate standards. The $\delta^{18}O$ and δD of water samples were determined at the USU Department of Geology Stable Isotope Laboratory using a ThermoScientific Delta V Advantage IRMS with a GasBench II interface. Oxygen and hydrogen isotope ratios were determined by continuous flow IRMS using CO_2 equilibration and H_2 equilibration with Pt reduction, respectively. Results are reported in per mil (‰) relative to SMOW based on in-house standards. $\delta^{18}O$ and δD uncertainties were ±0.06 ‰ and ±2.0 ‰, respectively, determined by repeat measurements of internal water standards calibrated to VSMOW and VSLAP, and replicate sample analyses.

Helium isotope ratios were measured at the Fluids and Volatiles Laboratory at Scripps Institution of Oceanography using gas extraction, purification, and analytical procedures described in Shaw et al. (2003). Measured $^{3}He/^{4}He$ ratios (R) are reported relative to air (R_A) which has a value of 1.4×10^{-6} (Ozima and Podosek, 1983). These ratios are corrected for atmospheric contamination of dissolved helium using $((R/R_A*X)-1)/(X-1)$ where X is the air-normalized He/Ne ratio multiplied by $ß_{Ne}/ß_{He}$, where $ß_{Ne}$ and $ß_{He}$ are the Bunsen solubility coefficients for neon and helium in pure water (Weiss, 1971; Hilton, 1996) at a temperature of 15 °C. Resulting air corrected values are reported as R_C/R_A in Table 1.

4. RESULTS AND DISCUSSION

4.1. Geochemistry of Cordillera Blanca Hot Springs

4.1.1. Aqueous Geochemistry and Geothermometry

The 8 hot spring locations investigated here range in temperature, pH, and specific conductance with values from 38 - 78 °C, 5.0 - 6.6, and 700 - 23,000 μS, respectively (Fig. 2, Table S2a). For comparison to the hot springs and to represent meteoric recharge infiltrating along the fault, cold springs, streams, and lakes were also sampled and analyzed during this study. Most thermal springs were degassing (bubbling) at their source (although this study focused on dissolved gas samples), and exhibited travertine accumulations. The springs emanate along a ~200 km NW-SE transect with flow paths through different geological units (phyllites, carbonates, and igneous rocks), and the aqueous chemistry can be explained by a binary mixture of an alkaline-chloride type saline groundwater with low salinity Ca - Na bicarbonate waters (Table S2b, Fig. S1). Local meteoric waters (e.g., Lochocota, Fig. S1) are Ca - Na bicarbonate type. Dissolved bicarbonate also follows this binary mixing trend (Fig. 3A). Notable trace elements include iron, arsenic (up to 10,800 ppb), thallium, antimony, and zinc (Table S2c).

Near-neutral, alkaline-chloride to alkaline-bicarbonate waters can provide reliable geothermal reservoir temperatures using Na-K and K-Mg geoindicators depending on the degree of equilibration between the water and the host rock mineralogy (Giggenbach, 1988). CB hot springs plot in the "partial equilibration" field of a ternary diagram comparing Na-K and K-Mg temperature calculations with estimates ranging from 200 - 275 and 72 - 174 °C, respectively (Fig. 4). For these samples, the Na-K results provide the best estimate of the higher temperature history of fluids; whereas, the K-Mg results are unreliable because they are susceptible to re-equilibration due to cooling and mixing with lower temperature ground waters. The results form a trend between partially equilibrated hot fluids and immature ground waters (Fig. 4), further supporting the interpretation that the hot springs represent mixing between deeply circulated saline fluids and shallow groundwater.

4.1.2. Stable Isotope Geochemistry ($\delta^{18}O$, δD, $\delta^{13}C$ and $^{3}He/^{4}He$)

Oxygen ($\delta^{18}O$) and hydrogen (δD) stable isotope ratios from the 8 hot spring locations range from -14.2 to -4.9 and -106.2 to -74.3 ‰ (SMOW), respectively (Fig. 3B, Table S3). We also report new $\delta^{18}O$ and δD values from 10 locations (streams, lakes, cold springs) in the Cordillera Blanca representative of local meteoric water located between 2600 and 4740 m above sea level (Fig 3B, Table S3). These meteoric water values are combined with those reported by Mark and McKenzie (2007) to define two local meteoric water lines (LMWL) (Fig. 3B LMWL *w* and *x*). Meteoric waters draining predominantly glaciated portions of the CB define a LMWL (*w*) with a slope of 6.7. Meteoric water (cold springs, streams) from the Cordillera Negra (non-glaciated) and the Rio Santa (Fig. 2) constrain a LMWL (*x*) with a shallower slope of 5.9.

The hot spring samples have stable isotope ratios that vary from similar to local meteoric water (either LMWL *w* or *x*) to significantly enriched in ^{18}O and ^{2}H with respect to LMW. Considered as a data set, the hot spring δD and $\delta^{18}O$ values form a linear trend (slope = 3.2) (Table S3, Fig. 3B *y*). This trend could be due to enrichment from a kinetic isotope effect driven by surface evaporation (Craig et al., 1963). In geothermal systems the $\delta^{18}O$ can be increased by high temperature exchange between meteoric water and silicate bedrock (Craig, 1963), and increases in both $\delta^{18}O$ and δD can be due to high temperature steam separation at depth (Giggenbach and Stewart, 1982), or mixing with brines equilibrated with metamorphic or igneous rocks at high temperatures (Sheppard, 1986). Near surface evaporation is unlikely to be important because these groundwater samples were collected at their discharge point at the surface; however, this process cannot be completely ruled out. Groundwater exchange with silicate bedrock causing increases in $\delta^{18}O$ would result in horizontal pathways from meteoric isotope compositions that are not represented in the current data set (Fig. 3B, e.g., path *z*). Steam separation at depth has been observed in other geothermal systems to produce similar trends (slope <3.6) in $\delta^{18}O$ and δD (Giggenbach and Stewart, 1982; Giggenbach, 1992). Groundwater mixing with isotopically distinct brines is also consistent with observed trends major ion chemistry (e.g., Fig. 3A). Thus, the plausible origins of the trend in hot spring isotope O and H ratios are mixing between meteoric recharge and brine, steam separation at depth, and possibly evaporation in the near surface.

Carbon stable isotope ratios of the total dissolved CO_2 ($\delta^{13}C_{CO2}$) range from -10.75 to -6.28 ‰ (Table 1, Fig. 5A). At Baños Huancarhuaz, the $\delta^{13}C$ of both the total dissolved CO_2 and exsolving CO_2 gas were measured at -10.75 and -14.49 ‰ (Table 1), respectively. This difference is larger than expected for equilibrium fractionation between these species at the

temperature and chemistry of this hot spring (3.74 vs. ~2.1 ‰), likely indicating some disequilibrium during degassing. Air-corrected $^{3}He/^{4}He$ ratios of dissolved gases in the springs vary from 0.62 to 1.98 R_A (Table 1). Using the highest air-corrected $^{3}He/^{4}He$ (1.98 R_A) value, this equates to ~25 % mantle-derived helium assuming a two-component mixture of a MORB mantle source (8 R_A) and crustal He (0.02 R_A)(Fig. 5A). This estimate would increase to 30 - 50% if helium originates from the continental mantle lithosphere (4 - 6 R_A) (Dodson et al., 1998; Gautheron and Moreira, 2002). Along volcanic arcs, the $CO_2/^{3}He$ ratio is used along with $\delta^{13}C_{CO2}$ to constrain the CO_2 source (Sano and Marty, 1995), and with $^{3}He/^{4}He$ to document mixing between mantle and crustal volatiles (O'Nions and Oxburgh, 1988). CB hot spring $CO_2/^{3}He$ ratios of dissolved gases vary from 6.09×10^{11} to 3.91×10^{13} (Table 1), and when combined with the $\delta^{13}C_{CO2}$ suggest a carbon source dominated by mixing of sedimentary (organic and carbonate) crustal sources (Fig. 5B). For example, applying a three-component mixing model using upper mantle ($\delta^{13}C$ = -6.5 ‰, $CO_2/^{3}He$ = 2×10^{9}), crustal organic sedimentary (-20 ‰ and 1×10^{13}), and crustal carbonate (0 ‰, 1×10^{13}) end-members (after Sano and Marty, 1995), the carbon at Baños Aquilina (Aq) is a mix of 54% organic sediments, 46% carbonates, and ~0.3% mantle-derived carbon. The $^{3}He/^{4}He$ and $CO_2/^{3}He$ ratios of CB hot springs plot on binary mixing curves between a mantle end member (8 R_A, 2×10^{9}) and a range of crustal end members (0.02 R_A, ~10^{13} - >10^{15}) (Fig. 5C). For a comparison to active volcanic arcs, published data from locations along the Andean Arc (Ecuador, and northern, central, and southern volcanic zones of Chile), Indonesia, and the Lesser Antilles are also plotted in Figure 5 (Table S1).

4.2. Modification of volatile geochemistry in the crust

The above analysis of $^{3}He/^{4}He$, $CO_2/^{3}He$, and $\delta^{13}C_{CO2}$ (Figs. 4A-C) assumes that mixing between mantle and different crustal reservoirs are the only processes controlling the dissolved gas ratios. However, mixing does not fully explain the inverse relationship displayed in Fig. 5D or the very low helium concentrations observed in some samples. In addition to mixing, modification of dissolved gas and stable isotope ratios due to degassing, gas dissolution, temperature variability, and mineralization is observed at active volcanic arcs (van Soest et al., 1998; Shaw et al., 2003; Ray et al., 2009) and a variety of continental settings (Gilfillan et al., 2009; de Leeuw et al., 2010). Similar inverse correlations between $CO_2/^{3}He$ and dissolved He at some active arc segments (Fig. 5D: SVZ Chile, Indonesia, and Lesser Antilles) has been interpreted as a degassing signal. Solubility differences between He and CO_2 lead to preferential He loss during degassing, resulting in the higher $CO_2/^{3}He$ ratios correlating with lower total dissolved He (van Soest et al., 1998). Degassing and loss of CO_2 in the geothermal system should also change the residual total dissolved CO_2 to higher $\delta^{13}C$ values, depending on the temperature, and the coupled variability in $CO_2/^{3}He$ and $\delta^{13}C$ observed in some active arc settings is attributed to both mixing and degassing (Fig. 5B). It is important to note that extensive carbonate mineralization during fluid ascent would lower the $CO_2/^{3}He$ ratio, have no impact on dissolved He, and depending on temperature, result in trends to lower residual $\delta^{13}C_{CO2}$ values.

To evaluate the impact of open system degassing on the observed CB hot spring $CO_2/^{3}He$ versus $\delta^{13}C_{CO2}$ and the $CO_2/^{3}He$ versus He relationships (Figs. 5B, D), we have applied the Rayleigh fractionation approach used in previous studies addressing degassing in geothermal systems related to volcanic arcs, active faults in continental settings, and at natural CO_2 gas domes (Gilfillan et al., 2009; Ray et al., 2009; de Leeuw et al., 2010). Our approach is summarized below:

Fractionation of the $CO_2/^3He$ ratio during progressive degassing is calculated using the following Rayleigh equation (e.g., Hilton et al., 1998; de Leeuw et al., 2010):

$$(CO_2/He)_f = (CO_2/He)_i \times F^{(\alpha-1)} \quad (1)$$

where *i* and *f* indicate the starting (initial) and residual CO_2/He of the dissolved gases in the hot spring water for some fraction (F, from 1 to 0) of the total helium remaining in solution. Alpha (α) is the temperature dependent fractionation factor between He and CO_2, and is the ratio of their solubility constants in water (He/CO_2). The solubility constant (Bunsen coefficient) for He in water at the desired temperature is calculated using Weiss (1971). We use the tabulations by Duan and Sun (2003) for the solubility of CO_2 in water as a function of temperature and pressure. Degassing fractionation between ^3He and ^4He is not considered due to the negligible solubility difference between these isotopes (Weiss, 1970), and the lack of inverse correlation between $^3He/^4He$ and He in this data set (Fig. S2).

Fractionation of carbon stable isotope ratios will also occur during progressive loss of $CO_{2(g)}$ through either degassing or through the precipitation of calcite, and can be modeled using the following form of the Rayleigh equation (Sharp, 2006).

$$\delta^{13}C_f = \delta^{13}C_i + (1000 + \delta^{13}C_i)(F^{(\alpha-1)}-1) \quad (2)$$

where *i* and *f* indicate the starting and residual $\delta^{13}C$ of the total dissolved CO_2 (total dissolved inorganic carbon, TDIC) in the spring water for some fraction (F, from 1 to 0) of the total carbon remaining in solution. Alpha (α) is the temperature dependent fractionation factor between $CO_{2(g)}$ and TDIC ($\alpha_{CO2(g)-TDIC}$) or between calcite and TDIC ($\alpha_{CC-TDIC}$). To accurately calculate $\alpha_{CO2(g)-TDIC}$, first the temperature dependent fractionation between the dissolved carbonate species and CO_2(g), $\varepsilon^{13}C_{TDIC-CO2(g)}$, is computed (Gilfillan et al., 2009):

$$\varepsilon^{13}C_{TDIC-CO2(g)} = x(\varepsilon^{13}C_{H2CO3(aq)-CO2(g)}) + (1-x)(\varepsilon^{13}C_{HCO3(aq)-CO2(g)}) \quad (3)$$

and,

$$\alpha_{CO2\text{-}DIC} = \exp^{(-\varepsilon 13C/1000)} \quad (4)$$

where x is the mole fraction of H_2CO_3(aq) and (1-x) is the mole fraction of HCO_3^-(aq). The temperature specific $\varepsilon^{13}C_{H2CO3(aq)\text{-}CO2(g)}$ and $\varepsilon^{13}C_{HCO3(aq)\text{-}CO2(g)}$ are calculated using the relationships in Deines et al. (1974). For the pH range (5 – 6.6) of the hot springs investigated, $CO_3^{2-}{}_{(aq)}$ is negligible and not considered. The dissolved carbonate speciation is calculated using PHREEQC (Parkhurst and Appelo, 1999) and the measured elemental chemistry, T, and pH of the spring water. The temperature specific fractionation factor between calcite and dissolved CO_2 is calculated using Bottinga (1968).

To evaluate how degassing and calcite mineralization may impact CB hot spring gas and isotope ratios, the spring with the highest dissolved He and lowest $CO_2/^3He$ ratio (Baños Aquilina, Fig. 5D "Aq") is used to represent the initial (*i*) condition in equations (1) and (2). Degassing curves for 78 and 180°C are plotted on Figures 5 B and D. This temperature range is chosen to represent degassing at the measured spring temperature (78°C) and higher temperatures (and pressures) occurring at depth. The solubility constant ratio (He/CO_2) at 78°C and 1 bar (surface) is 0.04, and 0.009 at 180°C and 100 bar (at depth). Note this range in temperature results only in a slight change in the degassing fractionation of the $CO_2/^3He$ ratio (Fig. 5D). In contrast, this temperature difference results in a significant difference in the fractionation of carbon isotope ratios during degassing. As shown by the two trajectories on Figure 5B, at 78°C the residual $\delta^{13}C_{CO2}$ becomes progressively higher, and at 180°C there is no fractionation. The horizontal arrow on Figure 5C is the degassing trajectory for $CO_2/^3He$, assuming no fractionation of the $^3He/^4He$ ratio. Figure 5B also shows calculated trajectories

starting at Aq due to calcite precipitation. $CO_2/^3He$ ratios decrease due to loss of CO_2 to calcite, and below ~180°C, carbon stable isotope ratios will decrease.

Based on this analysis, degassing provides a plausible explanation for some but not all of the trends in the data, and calcite mineralization results in trajectories that are inconsistent with the observed data. To aid in this discussion, three hot springs are circled on Figures 5B – D: Baños Aquilina (Aq), Huancarhuaz (Hc), and Olleros (Ol), which exhibit the highest and nearly identical $^3He/^4He$ ratios (1.79 to 1.98 R_A), the lowest and similar $\delta^{13}C_{CO2}$ (-10.75 to -10.30 ‰), but highly variable $CO_2/^3He$ ratios and dissolved He contents (6.09×10^{11} and 190 ncm^3STP/gH_2O to 3.91×10^{13} and 9.63 ncm^3STP/gH_2O). Figure 5B shows that degassing from the composition measured at Aq at high temperature (180°C) can explain the range of $CO_2/^3He$ and similar $\delta^{13}C$; however, lower temperature degassing (e.g., 78°C) would result in progressively higher $\delta^{13}C$ in Hc and Ol, which is not observed. Also, degassing from Aq to produce the $CO_2/^3He$ ratios at Hc and Ol (Fig 4C) provides a more plausible explanation than interpreting this distribution as mantle mixing with 3 very different crustal reservoirs ($CO_2/^3He$ ~10^{13} to >10^{15}). Finally, the inverse relationship between $CO_2/^3He$ and He and large range in dissolved He (Fig. 5D) is generally supported by degassing. However, the $CO_2/^3He$ ratios for Hc and Ol are higher than predicted by Rayleigh degassing alone from Aq. CO_2 addition along flow paths, or degassing from a different initial condition could explain this variability.

Compared to Aq, Hc, and Ol, the other CB hot springs characterized have a similar range of $CO_2/^3He$, but have higher and more variable $\delta^{13}C_{CO2}$ (-9.98 to -6.28 ‰) and lower $^3He/^4He$ ratios (0.62 to 1.33 R_A). The isotope geochemistry of these springs does not conform to a simple degassing scenario from the composition at Aq. Degassing is necessary to produce the observed

inverse relationship between $CO_2/^3He$ and He (Fig. 5D), but to explain the additional variability requires CO_2 addition, variable temperatures of degassing, and/or different initial conditions.

4.3. Cordillera Blanca detachment geothermal system

The trend in oxygen and hydrogen isotope ratios, mixing relationships in the major ion chemistry, elevated fluid temperature estimates from geothermometry, and the presence of elevated trace metal contents collectively support a mixture of shallow meteoric recharge with deeply circulated saline ground waters. The distribution of hot springs along the CB detachment fault zone is likely controlled by the location of individual subsurface hydrothermal groundwater cells and the permeability discontinuities between fault rocks and the host rocks (e.g., Forster and Smith, 1989). Here, we make a first-order estimate of the hydrothermal fluid circulation depth by using the maximum temperatures calculated using hot spring geothermometry (200-275°C), and applying a geothermal gradient of 25°C/km to suggest that ground waters may be circulating to depths of 8-11 km. Heat flow in the region is estimated to be low (McNulty and Farber, 2002); however, direct measurements near the CB detachment are not available. Thus, a locally higher thermal gradient associated with the CB detachment and batholith is possible and would decrease the fluid circulation depth estimate.

Based on the analysis in section 4.2, the isotope geochemistry of Baños Aquilina has experienced the least amount of crustal overprinting of the hot springs investigated. Thus, we hypothesize that the $^3He/^4He$, $CO_2/^3He$, and $\delta^{13}C_{CO2}$ values measured at this spring are the most representative of fluids moving from depth along the Cordillera Blanca detachment fault zone. In summary, hydrothermal fluids may be advecting from depths of 8-11 km, and carry a mix of mantle and crustal derived helium, with CO_2 derived primarily from carbonate and organic sedimentary crustal sources. The estimated proportions of mantle-derived helium and carbon are

~25% and ~0.3%, respectively. These estimates assume asthenospheric end-member compositions for He and C, and that degassing has not impacted the isotope geochemistry of Aq. The proportion of mantle-derived carbon would increase if Aq has been impacted significantly by degassing. Similarly, the fraction of mantle-derived helium would increase if values more consistent with the continental mantle-lithosphere were used as a mixing end-member.

4.4. Mantle helium in Cordillera Blanca detachment hydrothermal fluids

Possible origins for the mantle-derived helium in these hydrothermal fluids include residual fluids in the crust from earlier arc magmatism (>5 Ma), young fluids in the crust derived from a residual, thin mantle wedge or from upwelling asthenosphere accessing a tear in the flat slab (e.g., Antonijevic et al., 2015), or continental lithospheric mantle helium mobilized by metasomatic fluids released from the slab due to dehydration. Each of these possibilities will be considered with respect to available geophysical and geochemical constraints.

The most recent magmatic activity in the CB region was the eruption of a tuff at ca. 5.4 Ma that predates extension in the area, the formation of the Cordillera Blanca detachment fault, and unroofing of the CB massif (Giovanni et al., 2010). Regionally, this period of activity is interpreted to represent the waning stages of arc magmatism during the transition to flat-slab subduction. To evaluate if present-day $^{3}He/^{4}He$ ratios (~1.8 R_A) could be a residual stain from this magmatism, we have calculated the reduction of an original mantle ratio (8 R_A) due to radiogenic ^{4}He production in the crust, modifying the approach presented in Kulongoski et al., (2005).

$$^{4}He_{rad} = {}^{4}He_{prod} \times (1-\Phi)/\Phi \quad (5)$$

$$^{3}He/^{4}He_{r} = {}^{3}He_{m} / ({}^{4}He_{rad} \times t + {}^{4}He_{m}) \quad (6)$$

where $^4He_{rad}$ is the rate of ^4He production and accumulation in crustal pore fluids (mol gH_2O^{-1} yr^{-1}), $^4He_{prod}$ is the production rate for the crust (mol g^{-1} yr^{-1}), Φ is the porosity of the crustal rocks, $^3He/^4He_r$ is the present-day residual isotope ratio after ^4He ingrowth, ^3He_M and ^4He_M are the concentrations (mol g^{-1}) introduced by the magmatism, and t is years since the magmatic event. Assuming introduction of mantle fluids at 5.4 Ma, with a $^3He/^4He$ of 1.1×10^{-5} (8 R_A), ^4He of ~1300 ncm^3STP gH_2O^{-1} (4.1×10^{11} mol g^{-1}) based on average mantle values observed along the Chile SVZ (Fig. 5D, Table S1), average radiogenic production rates for ^4He in the crust (~1.6×10^{-17} mol g^{-1} yr^{-1}) (after Ballentine and Burnard, 2002), and a crustal porosity of 5%, the residual $^3He/^4He$ ratio from this event is estimated as 3.4×10^{-7} (0.25 R_A). This calculation does not consider the impact of mixing with the crustal helium reservoir that would further reduce the ratio. Therefore, radiogenic ingrowth of ^4He combined with mixing with meteoric groundwater would have long since diluted a mantle He signature from this magmatic pulse. For the observed ratios to be the product of mantle-derived magmatism, the event would need to have occurred <500 ka.

Mantle helium in crustal fluids in the absence of recent magmatism has been documented at major strike-slip faults such as the San Andreas Fault (Kennedy et al., 1997; Kulongoski et al., 2013), the Anatolian Fault (Güleç et al., 2002; Doğan et al., 2009; de Leeuw et al., 2010), and Karakoram Fault (Klemperer et al., 2013). In each case, the observed values require a continuous vertical fluid flux (<10 to 147 mm yr^{-1}) or much more rapid episodic flux of mantle helium from depth (Kennedy et al., 1997). The implication is that fluid pressures and permeability along these fault systems are high enough to move mantle-derived fluids from the asthenosphere through the ductile crust to the surface. Applying a similar model to the CB detachment is complicated for several reasons. In strike-slip settings, a near-vertical fault is presumably providing a pathway

from the asthenosphere to the shallow crust. However, the CB detachment is a low to moderate angle normal fault that penetrates to an unknown depth, but likely penetrates deep into the upper crust (McNulty and Farber, 2002). Additionally, the degassing documented in the CB springs complicates the flux calculation because it requires an estimate of the mantle-derived helium concentration, and estimating a pre-degassing He concentration is highly uncertain. However, we suggest that a similar magnitude of mantle helium flux must exist to transport these fluids into the CB detachment and produce the values observed in the CB hot springs. Based on this assessment, the question remains: is the mantle helium originating from underlying asthenosphere or from the mantle lithosphere?

Geophysical investigations (seismic and 2D tomography) constrain the general geometry and depth of flat slabs along the Andean margin (Gutscher et al., 2000). These authors show that the Peruvian flat slab beneath the CB region (~8.5 – 10 °S) has a depth of ~100 km, and is located in a broad 'sag' in the subducting plate observed between the Inca plateau and Nazca ridge. These geophysical data do not resolve the presence of asthenospheric mantle below the CB region. However, they have been interpreted to show slab steepening and 're-subduction' starting ~600 km east of the trench, and ~300 km east of the CB massif. The transition to steep subduction and appearance of an asthenospheric wedge in the north (~5 °S) and south (~15 °S) are 500-750 km from the CB massif (Gutscher et al., 2000). Using these geophysical constraints, mantle helium derived from an underlying residual or distal asthenospheric wedge is unlikely.

However, as presented in section 2.1, the recent higher resolution 3D seismic tomography of the Peruvian segment has identified a possible arc-parallel tear (Fig. 1) in the subducting slab north of the Nazca ridge between ~14 and 11 °S (Antonijevic et al., 2015). These results also indicate the presence of asthenosphere in the tear that is in contact with the continental

lithosphere. Antonijevic et al. (2015) hypothesize that the tear may continue to the north, but their data array does not extend far enough northward to constrain the presence of a tear or asthenosphere below the CB. Interestingly, these authors also note the presence of a localized high heat flow anomaly above the northern end of the asthenosphere filled tear. As mentioned previously, heat flow near the CB is considered low, but is based on sparse data (McNulty and Farber, 2002). Speculatively, the hydrothermal systems identified in our study along the CB detachment may be indicative of localized higher heat flow anomalies. Although direct supporting geophysical evidence is not available, it is possible that the mantle-helium observed in the CB region is related to a northward extension of the imaged slab tear and associated asthenosphere in contact with the lithosphere.

Another possible origin of the mantle helium observed in the CB hot springs is the continental mantle lithosphere, with He mobilized by fluids released from the subducting flat slab. Temperatures at the base of the continental lithosphere ~300 km from the trench in an established flat slab setting (> 5 Myr since closing of mantle wedge) are likely too low (~600°C) (Gutscher et al., 2000) to create melts, although aqueous/supercritical fluids will be released from the slab to the overlying lithosphere at these temperatures (e.g., Mungall, 2002). Due to the low angle of subduction, dehydration of the slab is likely to occur along the subduction interface for long distances inland from the trench (Pérez-Gussinyé et al., 2008; Jones et al., 2011). For example, dehydration of the Laramide-aged (late Cretaceous – early Tertiary) flat slab is postulated to have hydrated parts of the North American lithosphere for over 1000 km from the plate boundary (Humphreys et al., 2003; Jones et al., 2011). Additionally, mineral-fluid reactions (metasomatism) preserved in lower crustal (~40 km) xenoliths from the eastern parts of the North American Cordillera are attributed to fluid release from the Laramide flat slab, suggesting

that aqueous fluids derived from the mantle lithosphere were responsible for altering the lower crust (Jones et al., 2015). We suggest that continental mantle-lithosphere metasomatism during upward migration of slab-derived aqueous fluids is also a possible mechanism to release mantle-helium to deep fluids that then can migrate into shallow hydrothermal systems.

4.5. Transport of mantle-derived fluids through the lithosphere

Migration of slab-derived fluids across the brittle-ductile transition into the upper crust has been imaged above a newly forming subduction zone in New Zealand using magnetotelluric methods, and such fluids are hypothesized to be moving via developing fault-fracture meshes (Wannamaker et al., 2009). This mechanism is analogous to the fault-valve model that drives flow by fluid overpressurization and stress switching in a megathrust setting (Sibson, 2013). Similarly, Kennedy and van Soest (2007) argue that elevated levels of mantle-derived helium in the western U.S. are associated with high extensional and shear strain gradients that modify the permeability of the brittle-ductile transition, allowing movement of mantle-derived fluids into the shallow crust and associated brittle fault zones. Importantly, the formation of ore deposits has been attributed to metal-bearing fluids crossing the brittle-ductile transition via fracture systems during stress switching cycles in compressional settings, such as forearcs (e.g., Sibson, 2013). Mungall (2002) hypothesized that supercritical fluids (or melts) derived from subducting slabs can be sources of chalcophile elements in hydrothermal systems in flat slab settings. Our results further support these mechanisms for fluid transfer from mantle and slab depths into the brittle crust and to the surface, and show that this is a “plausible process”, even in settings with thick crust that lack active magmatism and associated conduits.

5. CONCLUSIONS

Here we document the presence of up to 25% mantle-derived helium in hot springs issuing from the Cordillera Blanca detachment fault system in a flat-slab subduction setting. These results begin to fill an important geochemical data gap for this unique tectonic setting. Recognition of mantle-derived fluids in this region of the Peruvian flat slab may represent the geochemical manifestation of migration of slab-derived fluids through the lithosphere, or the postulated tear in the slab and transition to steep subduction and the reestablishment of an asthenospheric wedge (Antonijevic et al., 2015). Our results provide support of existing ideas for the role of fluid dehydration from a flat slab in the subduction zone cycle. In this scenario, addition of mantle- and slab-derived fluids may weaken the continental lithosphere and impact deformation, uplift, and future magmatic activity, as hypothesized for ancient systems including the North American Cordillera (Humphreys et al., 2003; Jones et al., 2015) and the Altiplano – Puna plateau of the Andes (Hoke and Lamb, 2007; Garzione et al., 2008).

ACKNOWLEDGMENTS

Funding for this research was provided by Utah State University (Newell) and NSF-EAR-1220237 (Jessup and Shaw). Additionally, we thank J. Mauch for field support, the USU Water Research Laboratory (J. McLean) for assistance in elemental analysis, and A. Cafferata in Caraz, Peru for field logistical support. We thank Dr. Franco Tassi and an anonymous reviewer for their thoughtful reviews and suggestions that improved this manuscript.

TABLES

Table 1. Cordillera Blanca hot spring $^3He/^4He$ ratios, and carbon isotope ratios of CO_2

Spring (Baños)	Sample ID	R/R_A	$X^{\#}$	$R_C/R_A^{\S}$ ($\pm1\sigma$)	$CO_2/^3He$ ($x10^{12}$)	$[^4He]_m$ (cm^3STP/gH_2O)	$[^4He]_c^*$ (cm^3STP/gH_2O)	$\delta^{13}C_{CO2}^{**}$ (‰) PDB
Olleros	CB05	1.05	5.43	1.06 ±0.24	10.3	7.08E-08	5.77E-08	-7.82
Olleros	CB06	1.8	36.9	1.82 ±0.55	39.1	9.89E-09	9.63E-09	-10.30
Merced	CB07	0.7	5.07	0.62 ±0.17	27.3	2.40E-08	1.93E-08	-6.28
Chancos	CB08a	1.24	3.65	1.33 ±0.31	4.22	4.18E-08	3.03E-08	-9.06
Chancos	CB08b	0.9	3.51	0.85 ±0.24	19.2	3.32E-08	2.38E-08	-9.72
Monterrey	CB09	1.27	13.2	1.30 ±0.30	2.44	1.10E-07	1.02E-07	-9.96
Huancarhuaz -g	CB11g	1.95	36.7	1.98 ±0.40	0.269	-	-	-14.49
Huancarhuaz	CB11	1.66	5.28	1.81 ±0.46	6.85	7.08E-08	5.77E-08	-10.75
Aquilina	CB14	1.78	53.7	1.79 ±0.40	0.609	1.94E-07	1.90E-07	-10.74

g - gas Sample; all others water samples

$^{\#}$ $X = (^4He/^{20}Ne)_{measured}/(^4He/^{20}Ne)_{air}$ x βNe/ βHe; β = Bunsen coefficient from (Weiss, 1971): groundwater recharge temperature of 15ºC.

§ R_C/R_A is the air-corrected He isotope ratio = $[(R_m/R_A \text{ x } X)-1]/(X-1)$. R_m is measured $^3He/^4He$ ratio divided by the $^3He/^4He$ in air ($R_A = 1.4 \text{ x } 10^{-6}$)

*Dissolved He concentrations are air-corrected where $[He]_C = ([He]_m \text{ x } (X-1))/X$

$^{**}\delta^{13}C$ errors are estimated at ±0.10 ‰ based on repeat NBS standard runs

FIGURE CAPTIONS

Figure 1. Andean arc showing current flat slab segments, the locations of subducted oceanic ridges and plateaux (Gutscher et al., 2000), and slab depth contours (km) based on earthquake depths (Antonijevic et al., 2015) along the present-day location of the Nazca ridge. $^3He/^4He$ results (air-corrected) from this study are shown in the box compared to a compilation of published data from the Andes (see Table S-1 for data and citations). The extent of the Altiplano – Puna plateau is based on Allmendinger et al. (1997). (2 Column Figure, color in print + on-line)

Figure 2. Hot springs of the Cordillera Blanca investigated during this study. Results shown include measured temperature, the Na-K temperature estimates in parenthesis, the air-corrected $^3He/^4He$ (R_C/R_A) values, and As concentration (ppb). Surface geology modified from Giovanni et al. (2010). (1.5 Column Figure, color in print + on-line)

Figure 3. A) Cross plot of dissolved HCO_3^- versus dissolved Cl^-. These data are interpreted as representing mixing between saline and dilute end-members. B) $\delta^{18}O$ and δD of CB hot springs and local, cold meteoric water from this study and Mark and McKenzie (2007). Local meteoric water lines and *x* are defined by meteoric waters from the glaciated Cordillera Blanca (*w*, r^2=0.75) and the Rio Santa and non-glaciated Cordillera Negra (*x*, r^2=0.98); GMWL – global meteoric water line (Craig, 1961). CB hot springs fall on trend *y* (slope 3.2, r^2=0.85). Included on the plot are the isotope compositions of "metamorphic fluids" (Sharp, 2006) and 'andesite water' (Giggenbach, 1992). (1 column figure)

Figure 4. Ternary diagram combining the Na-K and K-Mg geothermometers (modified from Giggenbach, 1988). The two thermometers intersect at the same temperature along the 'Full Equilibration Line'. The Baños Olleros, Huancarhuaz, and Monterrey samples plot on the 260°C Na-K isotherm within the 'Partial Equilibration' field. Baños Aquilina falls on the 200°C Na-K isototherm. (1 column figure, on-line color only)

Figure 5. A) $^3He/^4He$ (R/R_A, uncorrected for air contribution) vs. He/Ne mixing diagram showing the CB hot springs (diamonds) compared to Baños Toros in the Chilean flat slab, and other Andean arc data (Table S-1). End members include ASW (air saturated water; 1 R_A, He/Ne

= 0.32), Crust (0.02 R_A, He/Ne >1000), and Mantle (8 R_A, He/Ne > 1000). B) $CO_2/^3He$ vs. $\delta^{13}C_{CO2}$ mixing diagram between mantle, crustal sedimentary (organic), and crustal carbonate – derived CO_2 end-members (after Sano and Mary, 1995). CB hot springs (diamonds) plot as a mixture of crustal sedimentary and carbonate sources with minor mantle contributions. Baños Aquilina (Aq), Baños Huancarhuaz (Hc), and Baños Olleros (Ol) are highlighted to guide discussions in text. Open system degassing trajectories (dashed arrows, with percent degassed shown) originate from Aq showing how degassing at 78 and 180°C modifies the $CO_2/^3He$ ratio and $\delta^{13}C_{CO2}$ values of residual dissolved gases (see text for details of degassing model). Also shown are trajectories originating from Aq for the residual fluid composition due to progressive calcite precipitation at 78 and ~180°C. Hc_w and Hc_g are dissolved gas in water and free gas samples, respectively. C) $^3He/^4He$ (R_C/R_A) vs. $CO_2/^3He$ for CB hot springs (diamonds). Also shown are binary mixing curves between a mantle end-member (8 R_A and 2×10^9) and a range of crustal end-members (0.02 R_A, and $CO_2/^3He$ $10^{10} – 10^{15}$). The horizontal dashed line from Aq to Ol indicates how degassing impacts $CO_2/^3He$ ratios. D) $CO_2/^3He$ vs. dissolved He showing inverse relationship in CB hot springs data (diamonds). Open system degassing from Aq for 78 and 180°C are shown as dashed lines (see text for details of model). Also included on panels B, C, and D are representative data from active arcs including the Andes (Ecuador, Northern Chile, Central Chile, and the Chile Southern Volcanic Zone – SVZ), Indonesia, and Lesser Antilles (see Table S1 for data and citations). (2 column figure)

REFERENCES

Allmendinger, R. W., Jordan, T. E., Kay, S. M., and Isacks, B. L., 1997, The evolution of the Atliplano-Puna plateau of the central Andes: Annual Review of Earth and Planetary Sciences, v. 25, p. 139-174.

Antonijevic, S. K., Wagner, L. S., Kumar, A., Beck, S., Long, M. D., Zandt, G., Tavera, H., and Condori, C., 2015, The role of ridges in the formation and longevity of flat slabs: Nature, v. 524, p. 212-215.

Atherton, M. P., and Sanderson, L. M., 1987, The Cordillera Blanca batholith: a study of granite intrusion and the relation of crustal thickening to peraluminisity: Geologische Rundschau, v. 76, p. 213-232.

Ballentine, C. J., and Burnard, P. G., 2002, Production, release and transport of noble gases in the continental crust, *in* Porcelli, D., Ballentine, C. J., and Weiler, R., eds., Reviews in Mineralogy & Geochemistry - Noble Gases in Geochemistry and Cosmochemistry, Volume 47: Washington D.C., Mineralogical Society of America, p. 481-538.

Bottinga, Y., 1968, Calculation of fractionation factors for carbon and oxygen isotopic exchange in the system calcite-carbon dioxide - water: Journal of Physical Chemistry, v. 72, p. 800-807.

Craig, H., 1961, Isotopic variations in meteoric waters: Science, v. 133.

-, 1963, The isotope geochemistry of water and carbon in geothermal areas, *in* Tongiorgi, E., ed., Nuclear Geology on Geothermal Areas: Pisa, Italy, p. 17-53.

Craig, H., Gordon, L. I., and Horibe, Y., 1963, Isotopic exchange effects in the evaporation of water: Journal of Geophysical Research, v. 68, p. 5079-5087.

de Leeuw, G. A. M., Hilton, D. R., Güleç, N., and Mutlu, H., 2010, Regional and temporal variations in $CO_2/^3He$, $^3He/^4He$ and $\delta^{13}C$ along the North Anatolian Fault Zone, Turkey: Applied Geochemistry, v. 25, p. 524-539.

Deines, P., Langmuir, D., and Harmon, R. S., 1974, Stable carbon isotope ratios and the existence of a gas phase in the evolution of carbonate ground waters: Geochimica et Cosmochimica Acta, v. 38, p. 1147-1164.

Dodson, A., DePaolo, D. J., and Kennedy, B. M., 1998, Helium isotopes in the lithospheric mantle: Evidence from Tertiary basalts of the western USA: Geochimica et Cosmochimica Acta, v. 62, p. 3775-3787.

Doğan, T., Sumino, H., Nagao, K., Notsu, K., Tuncer, M. K., and Çelik, C., 2009, Adjacent releases of mantle helium and soil CO2 from active faults: Observations from the Marmara region of the North Anatolian Fault zone, Turker: Geochemisty, Geophysics, and Geosystems, v. 10, p. 1 - 11.

Duan, Z., and Sun, R., 2003, An improved model calculating CO_2 solubility in pure water and aqueous NaCl solutions from 273 to 533 K and from 0 to 2000 bar: Chemical Geology, v. 193, p. 257-271.

Fischer, T., Hilton, D., Zimmer, M. M., Shaw, A. M., Sharp, Z., and Walker, J. A., 2002, Subduction and recycling of nitrogen along the Central American margin: Science, v. 297, p. 1154-1157.

Forster, C. B., and Smith, L., 1989, The influence of groundwater flow on thermal regimes in mountainous terrain: A model study: Journal of Geophysical Research, v. 94, p. 9439-9451.

Garzione, C. N., Hoke, G. D., Libarkin, J. C., Withers, S., MacFadden, B., Eiler, J. M., Ghosh, P., and Mulch, A., 2008, Rise of the Andes: Science, v. 320, p. 1304-1307.

Gautheron, C., and Moreira, M., 2002, Helium signature of the subcontinental lithospheric mantle: Earth and Planetary Science Letters, v. 199, p. 39-47.

Giggenbach, W. F., 1988, Geothermal solute equilibria. Derivation of Na-K-Mg-Ca geoindicators: Geochimica et Cosmochimica Acta, v. 52, p. 2749-2765.

-, 1992, Isotopic shifts in waters from geothermal and volcanic systems along convergent plate boundaries and their origin: Earth and Planetary Science Letters, v. 113, p. 495-510.

Giggenbach, W. F., and Stewart, M. K., 1982, Processes controlling the isotopic composition of steam and water discharges from steam vents and steam heated pools in geothermal areas: Geothermics, v. 11, p. 71-80.

Gilfillan, S. M. V., Sherwood Lollar, B., Holland, G., Blagburn, D., Stevens, S., Schoell, M., Cassidy, M., Ding, Z., Zhou, Z., Lacrampe-Couloume, G., and Ballentine, C. J., 2009, Solubility trapping in formation water as dominant CO_2 sink in natural gas fields: Nature, v. 458, p. 614-617.

Giovanni, M. K., Horton, B. K., Garzione, C. N., McNulty, B., and Grove, M., 2010, Extensional basin evolution in the Cordillera Blanca, Peru: Stratigraphic and isotopic records of detachment faulting and orogenic collapse in the Andean hinterland: Tectonics, v. 29, p. 1-21.

Güleç, N., Hilton, D. R., and Multu, H., 2002, Helium isotope variations in Turkey: relationship to tectonics, volcanism and recent seismic activities: Chemical Geology, v. 187, p. 129-142.

Gutscher, M.-A., Spakman, W., Bijwaard, H., and Engdahl, E. R., 2000, Geodynamics of flat subduction: Seismicity and tomographic constraints from the Andean margin: Tectonics, v. 19, no. 5, p. 814-833.

Hilton, D., Fischer, T. P., and Marty, B., 2002, Noble gases and volatile recycling at subduction zones, *in* Porcelli, D., Ballentine, C. J., and Weiler, R., eds., Reviews in Mineralogy & Geochemistry - Noble Gases in Geochemistry and Cosmochemistry, Volume 47: Washington D.C., Mineralogical Society of America, p. 319-370.

Hilton, D. R., 1996, The helium and carbon isotope systematics of a continental geothermal system: results from monitoring studies at Long Valley caldera (California, USA): Chemical Geology, v. 127, no. 4, p. 269-295.

Hilton, D. R., Hammerschmidt, K., Teufel, S., and Friedrichsen, H., 1993, Helium isotope characteristics of Andean geothermal fluids and lavas: Earth and Planetary Science Letters, v. 120, p. 265-282.

Hilton, D. R., McMurty, G. M., and Goff, F., 1998, Large variations in vent fluid $CO_2/^3He$ ratios signal rapid changes in magma chemistry at Loihi seamount, Hawaii: Nature, v. 396, p. 359-362.

Hoke, L., and Lamb, S., 2007, Cenozoic behind-arc volcanism in the Bolivian Andes, South America: implications for mantle-melt generation and lithospheric structure: Journal of the Geological Society, v. 164, p. 795-814.

Huaccan, A. H., 2000, Aguas termales y minerales en el norte del Peru, Bolentin No 22: Instituto Geologico Minero Y Metalurgico.

Humphreys, E., Hessler, E., Dueker, K., Farmer, G. L., Erslev, E., and Atwater, T., 2003, How Laramide-age hydration of North American lithosphere by the Farallon Slab controlled subsequent activity in the Western United States: International Geology Review, v. 45, no. 7, p. 575-595.

Jones, C. H., Framer, G. L., Sageman, B., and Zhong, S., 2011, Hydrodynamic mechanism for the Laramide orogeny: Geosphere, v. 7, p. 183-201.

Jones, C. H., Mahan, K. H., Butcher, L. A., Levandowski, W. B., and Farmer, L., 2015, Continental uplift through crustal hydration: Geology, v. 43, p. 355-358.

Kay, S. M., and Abbruzzi, J. M., 1996, Magmatic evidence for Neogene lithospheric evolution of the central Andean "flat-slab" between 30°S and 32°S: Tectonophysics, v. 259, p. 15-28.

Kennedy, B. M., Kharaka, Y. K., Evans, W. C., Ellwood, A., DePaolo, D. J., Thordsen, J., Ambats, G., and Mariner, R. H., 1997, Mantle Fluids in the San Andreas Fault System, California: Science, v. 278, p. 1278-1281.

Kennedy, B. M., and van Soest, M. C., 2007, Flow of mantle fluids through the ductile lower crust: Helium isotope trends: Science, v. 318, p. 1433-1436.

Klemperer, S. L., Kennedy, B. M., Sasty, S. R., Makovsky, Y., Harinarayana, T., and Leech, M. L., 2013, Mantle fluids in the Karakoram fault: Helium isotope evidence: Earth and Planetary Science Letters, v. 366, p. 59-70.

Kulongoski, J. T., Hilton, D. R., Barry, P. H., Esser, B. K., Hillegonds, D., and Belitz, K., 2013, Volatile fluxes through the Big Bend section of the San Andreas Fault, California: Helium and carbon-dioxide systematics: Chemical Geology, v. 339, p. 92-102.

Kulongoski, J. T., Hilton, D. R., and Izbicki, J. A., 2005, Source and movement of helium in the eastern Morongo groundwater Basin: The influence of regional tectonics on crustal and mantle helium fluxes: Geochimica et Cosmochimica Acta, v. 69, no. 15, p. 3857-3872.

Lee, C.-T. A., 2005, Trace element evidence for hydrous metasomatism at the base of the North American lithosphere and possible association with Laramide low-angle subduction: The Journal of Geology, v. 113, p. 673-685.

Mark, B. G., and McKenzie, J. M., 2007, Tracing increasing tropical Andean glacier melt with stable isotopes in water: Environmental Science & Technology, v. 41, p. 6955-6960.

McNulty, B., and Farber, D., 2002, Active detachment faulting above the Peruvian flat slab: Geology, v. 30, p. 567-570.

Meqbel, N. M., Egber, G. D., Wannamaker, P. E., Kelbert, A., and Schultz, A., 2014, Deep electrical resistivity structure of the northwestern U.S. derived from 3-D inversion of USArray magnetotelluric data: Earth and Planetary Science Letters, v. 402, p. 290-304.

Mungall, J. E., 2002, Roasting the mantle: Slab melting and the genesis of major Au an Au-rich Cu deposits: Geology, v. 30, p. 915-918.

O'Nions, R. K., and Oxburgh, E. R., 1988, Helium, volatile fluxes and the development of continental crust: Earth and Planetary Science Letters, v. 90, p. 331-347.

Ozima, M., and Podosek, F., 1983, Noble gas geochemistry, Cambridge, United Kingdom, Cambridge Univ. Press, 377 p.:

Parkhurst, D. L., and Appelo, C. A. J., 1999, User's guide to PHREEQC (Version 2)-A computer program for speciation, batch-reaction, one-dimensional transport, and inverse geochemical calculations: USGS Water-Resources Investigations Report 99-4259, p. 310.

Peacock, S. M., 1990, Fluid processes in subduction zones: Science, v. 248, p. 329-337.

Pérez-Gussinyé, M., Lowry, A. R., Morgan, J. P., and Tassara, A., 2008, Effective elastic thickness variations along the Andean margin and their relationship to subduction geometry: Geochemisty, Geophysics, and Geosystems, v. 9, p. 1-21.

Pilger, R. H., 1981, Plate reconstructions, aseismic ridges, and low-angle subduction beneath the Andes: Geological Society of America Bulletin, v. 92, p. 448-456.

Ramos, V. A., and Folguera, A., 2009, Andean flat-slab subduction through time, *in* Murphy, J. B., Keppie, J. D., and Hynes, A. D., eds., Ancient Orogens and Modern Analogues, Geological Society, London, Special Publications, Volume 327, p. 31-54.

Ray, M. C., Hilton, D. R., Muñoz, J., Fischer, T. P., and Shaw, A. M., 2009, The effects of volatile recycling, degassing and crustal contamination on the helium and carbon

geochemistry of hydrothermal fluids from the Southern Volcanic Zone of Chile: Chemical Geology, v. 266, p. 38-49.

Sano, Y., and Marty, B., 1995, Origin of carbon in fumarolic gas from island arcs: Chemical Geology, v. 119, p. 265-274.

Scambelluri, M., and Philippot, P., 2001, Deep fluids in subduction zones: Lithos, v. 55, p. 213-227.

Sharp, Z. D., 2006, Principles of Stable Isotope Geochemistry, Upper Saddle River, N.J., Pearson/Prentice Hall, 344 p.:

Shaw, A. M., Hilton, D. R., Fischer, T. P., Walker, J. A., and Alvarado, G., 2003, Contrasting volatile systematics of Nicaragua and Costa Rica: insights to C-cycling through subduction zones: Earth and Planetary Science Letters, v. 214, no. 3-4, p. 499-513.

Sheppard, S. M. F., 1986, Characterization and isotopic variations in natural waters, *in* Valley, J. W., Taylor, H. P., and O'Neil, J. R., eds., Stable Isotopes in High Temperature Geological Processes, Volume 16: Chelsea, MI, Mineralogical Society of America, p. 165-183.

Sibson, R. H., 2013, Stress switching in subduction forearcs: Implications for overpressure containment and strength cycling on megathrusts: Tectonophysics, v. 600, p. 142-152.

van Soest, M. C., Hilton, D. R., and Kreulen, R., 1998, Tracing crustal and slab contribution to arc magmatism in the Lesser Antilles island arc using helium and carbon relationships in geothermal fluids: Geochimica et Cosmochimica Acta, v. 62, no. 19/20, p. 3323-3335.

Wannamaker, P. E., Caldwell, T. G., Jiracek, G. R., Maris, V., HIll, G. J., Ogawa, Y., Bibby, H. M., Bennie, S. L., and Heise, W., 2009, Fluid and deformation regime of an advancing subduction system at Marlborough, New Zealand: Nature, v. 460, p. 733-736.

Weiss, R. F., 1970, Helium isotope effect in solution in water and seawater: Science, v. 168, p. 247-248.

-, 1971, Solubility of helium and neon in water and seawater: Journal of Chemical and Engineering Data, v. 16, no. 2, p. 235-241.

Zandt, G., Leidig, M., Chmielowski, J., Baumont, D., and Yuan, X., 2003, Seismic detection and characterization of the Altiplano-Puna magma body, Central Andes: Pure and Applied Geophysics, v. 160, p. 789-807.

Zimmer, M. M., Fischer, T. P., Hilton, D. R., Alvarado, G. E., Sharp, Z. D., and Walker, J. A., 2004, Nitrogen systematics and gas fluxes of subduction zones: Insights from Costa Rica arc volatiles: Geochemistry, Geophysics, Geosystems, v. 5, no. 5.

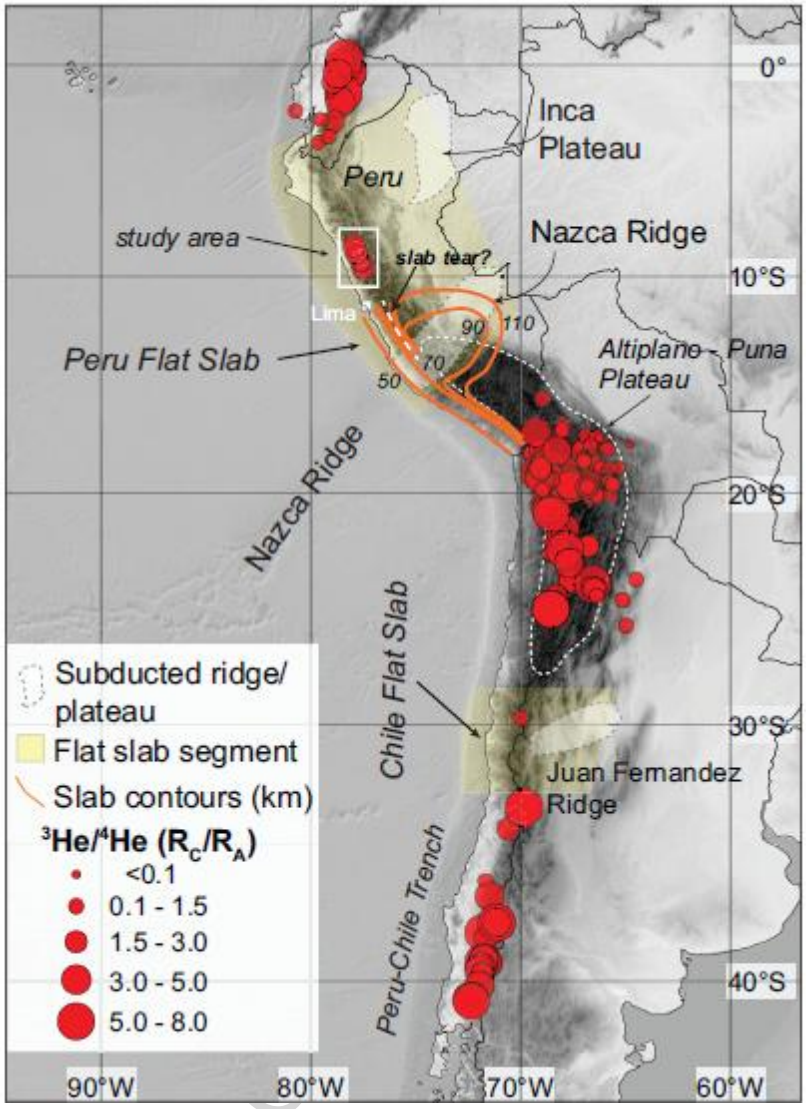

Figure 1

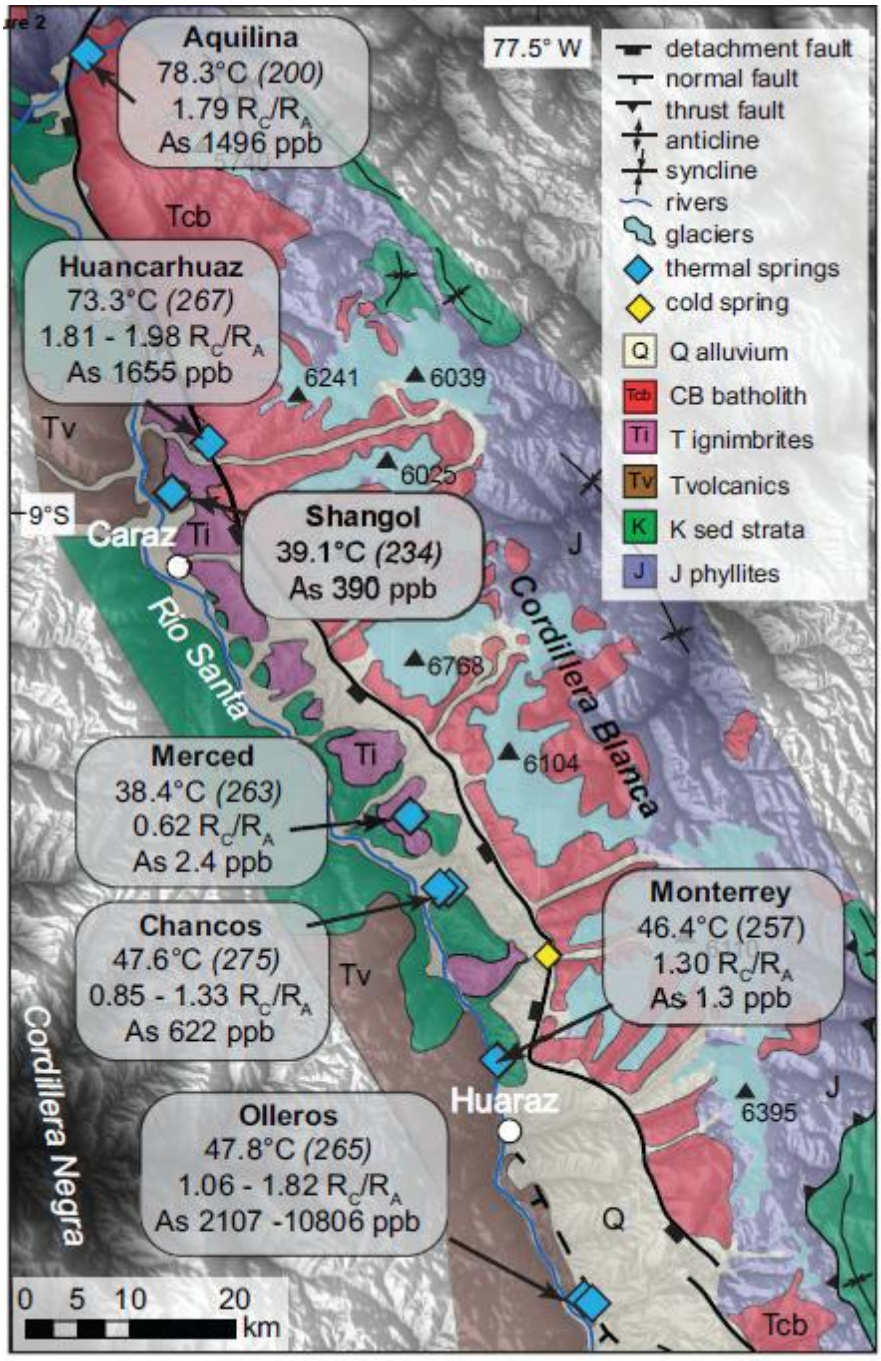
Aquilina
78.3°C (200)
1.79 R_C/R_A
As 1496 ppb
Tcb
Huancarhuaz
73.3°C (267)
1.81 - 1.98 R_C/R_A
As 1655 ppb
6241
6039
Tv
6025
9°S
Caraz
Ti
Shangol
39.1°C (234)
As 390 ppb
J
Rio Santa
Cordillera Blanca
6768
Ti
6104
Merced
38.4°C (263)
0.62 R_C/R_A
As 2.4 ppb
Monterrey
46.4°C (257)
1.30 R_C/R_A
As 1.3 ppb
Chancos
47.6°C (275)
0.85 - 1.33 R_C/R_A
As 622 ppb
Tv
Cordillera Negra
Huaraz
6395
J
Olleros
47.8°C (265)
1.06 - 1.82 R_C/R_A
As 2107 -10806 ppb
Q
0 5 10 20
km
Tcb
77.5° W
detachment fault
normal fault
thrust fault
anticline
syncline
rivers
glaciers
thermal springs
cold spring
Q Q alluvium
Tcb CB batholith
Ti T ignimbrites
Tv Tvolcanics
K K sed strata
J J phyllites

Figure 2

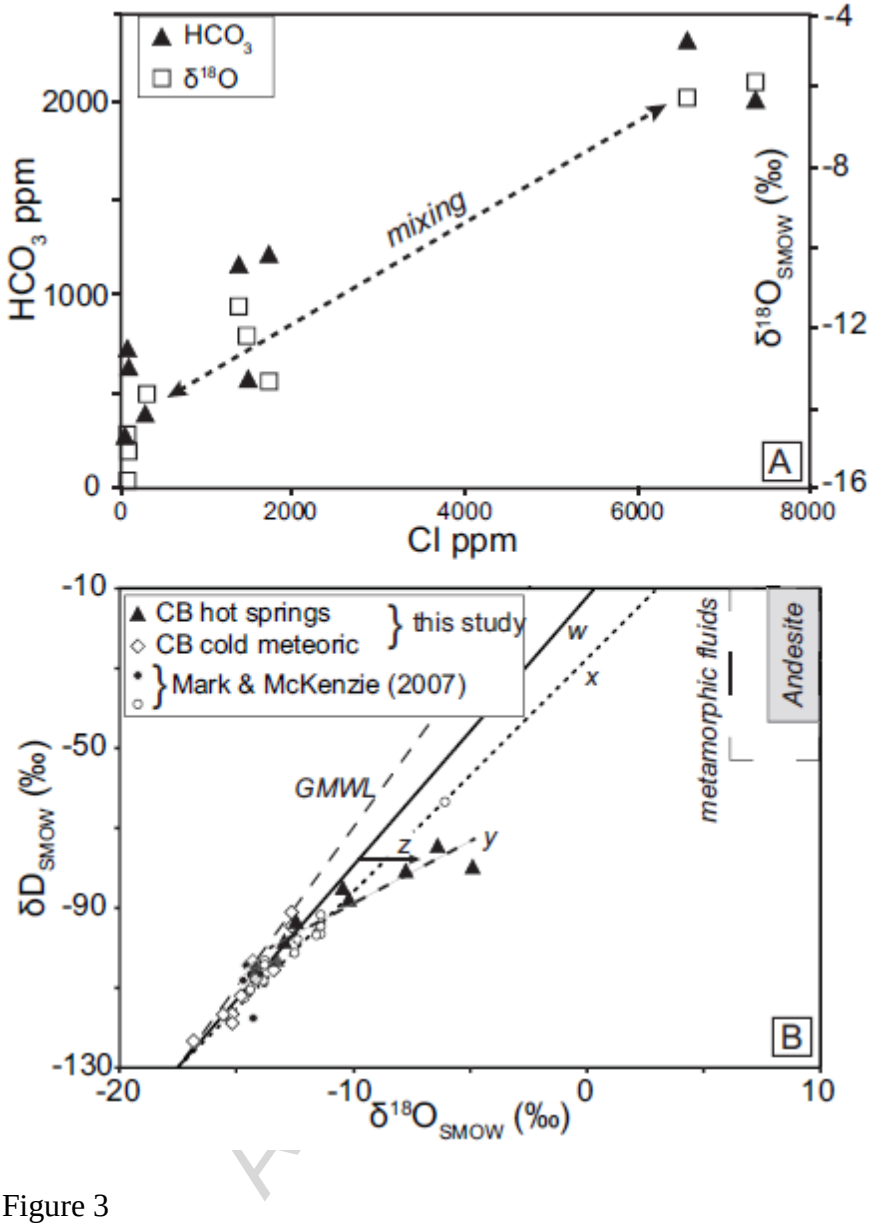

Figure 3

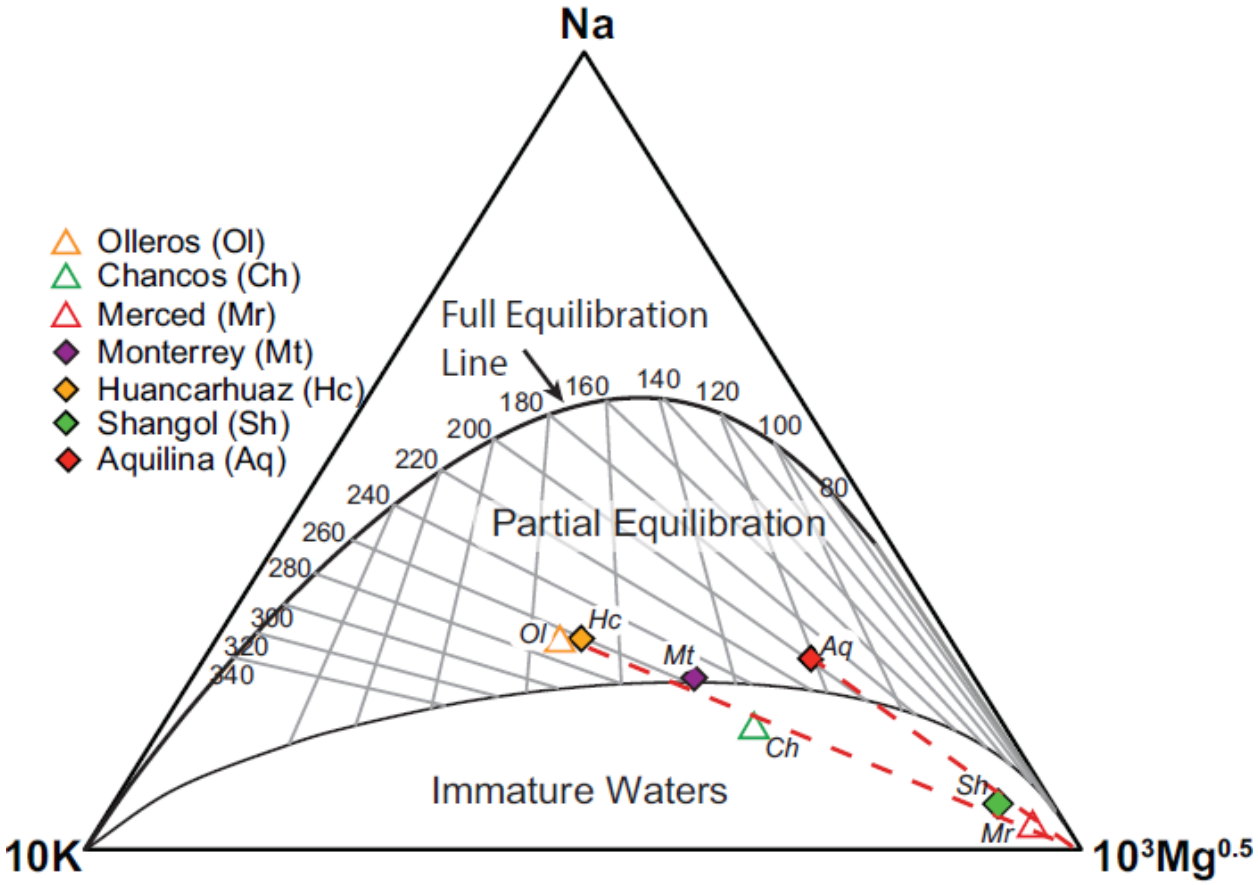

Figure 4

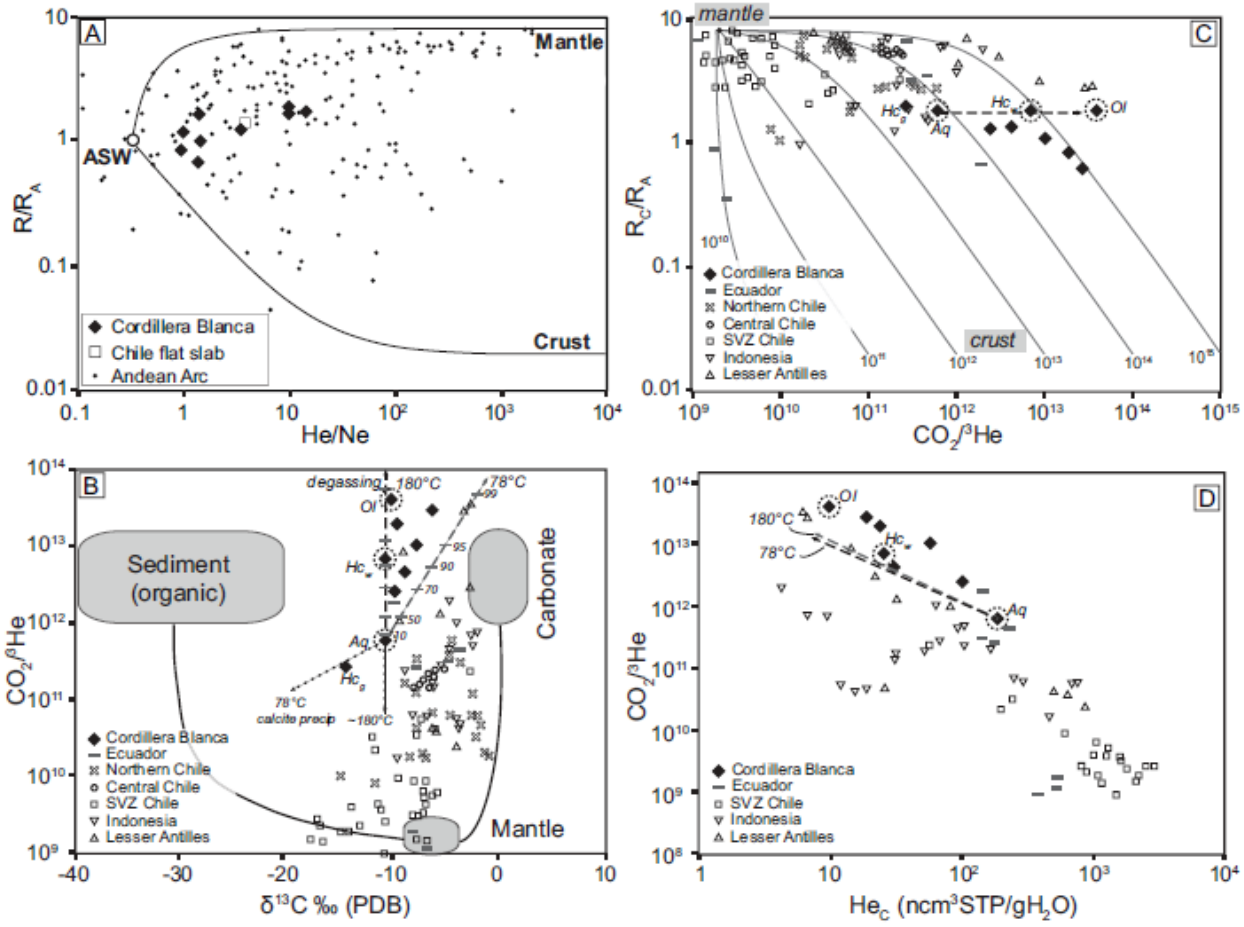

Figure 5

Mantle-derived helium in hot springs of the Cordillera Blanca, Peru: implications for mantle-to-crust fluid transfer in a flat-slab subduction setting

Dennis L. Newell, Micah J. Jessup, David R. Hilton, Colin Shaw, and Cameron Hughes

Highlights

Mantle volatile signal detected in hot spring geochemistry from the Cordillera Blanca, Peru, above amagmatic flat slab

Mantle helium may be the shallow geochemical manifestation of tear in Peruvian flat slab

Hydrothermal groundwater circulation to 11 km in Cordillera Blanca detachment fault

Hot springs carry elevated dissolved metals, including up to 11 ppm arsenic